Fig S1

A

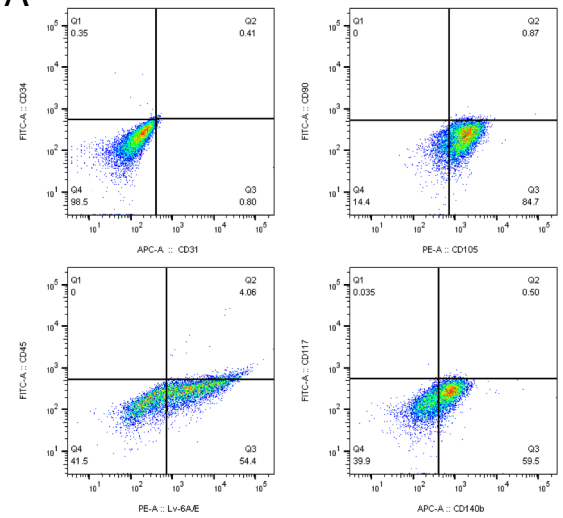
Q1
0.35
Q2
0.41
Q4
98.5
Q3
0.80
FITC-A :: CD34
APC-A :: CD31
Q1
0
Q2
0.87
Q4
14.4
Q3
84.7
FITC-A :: CD90
PE-A :: CD105
Q1
0
Q2
4.06
Q4
41.5
Q3
54.4
FITC-A :: CD45
PE-A :: Ly-6A/E
Q1
0.035
Q2
0.50
Q4
39.9
Q3
59.5
FITC-A :: CD117
APC-A :: CD140b

B

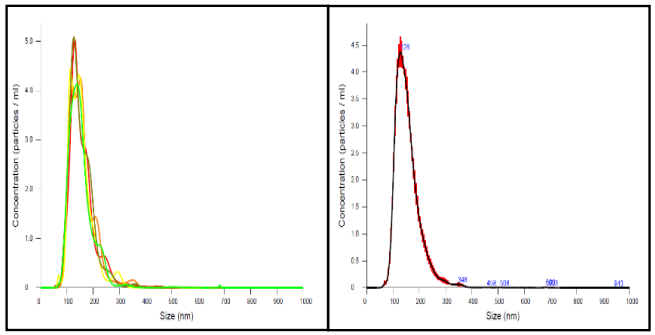
Concentration (particles / ml)
Size (nm)
Concentration (particles / ml)
Size (nm)

C

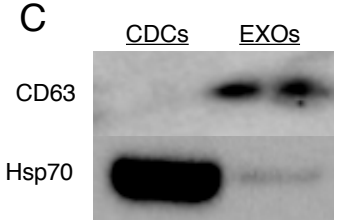
CDCs
EXOs
CD63
Hsp70

Figure S1. Characterization of Mouse CDCs and Human EXOs. (**A**) Representative flow cytometry dot plot indicating the abundance of selected surface markers. CDCs are negative for hematopoietic surface makers and positive for known CDC surface antigens. (B) Representative histogram from nanoparticle tracking analysis using dynamic light scattering to measure exosome concentration and size. (C) Immunoblot for common exosomal markers from CDCs and their exosomes.

Fig S2

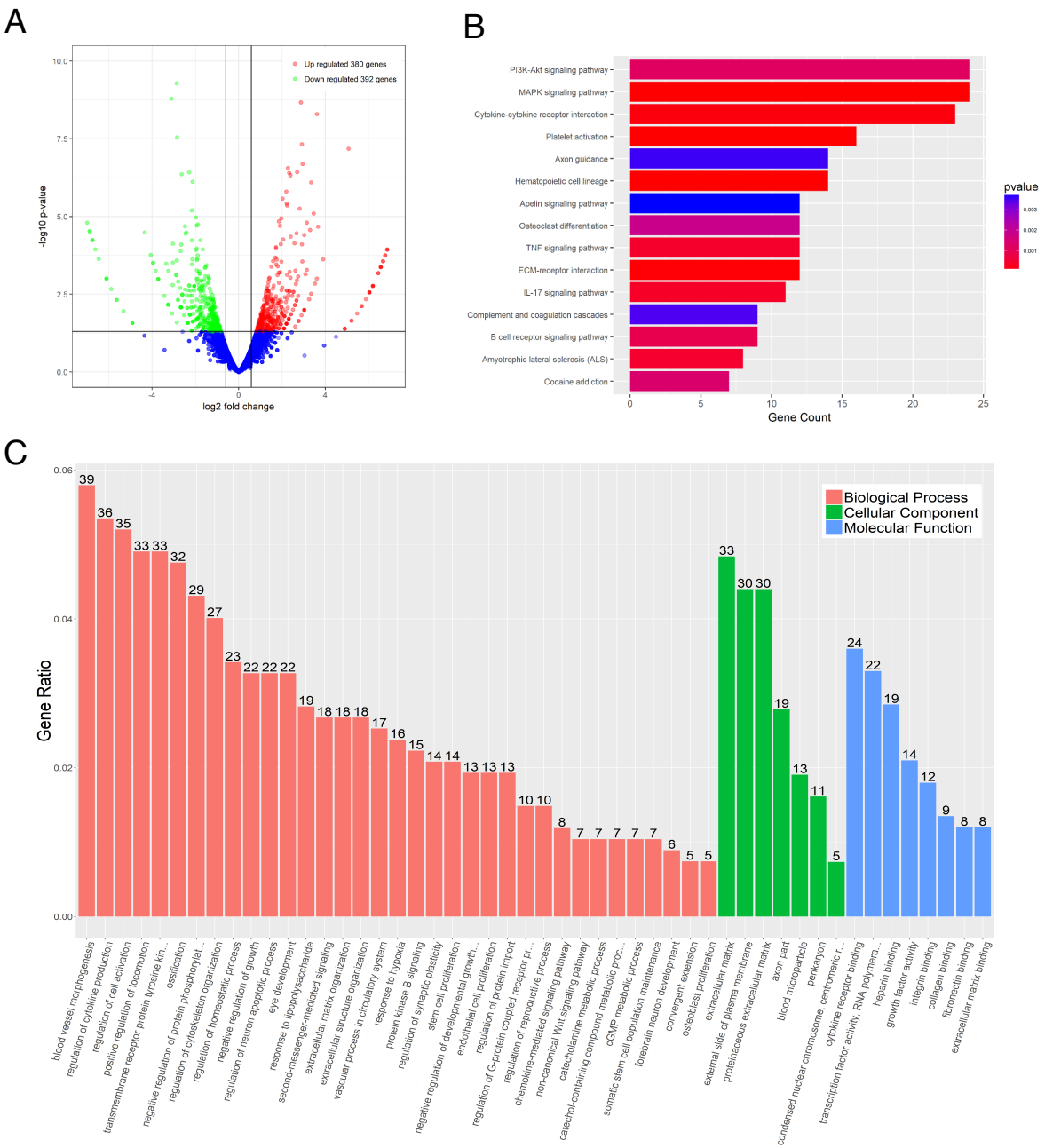
A
Up regulated 380 genes
Down regulated 392 genes
-log10 p-value
log2 fold change
B
PI3K-Akt signaling pathway
MAPK signaling pathway
Cytokine-cytokine receptor interaction
Platelet activation
Axon guidance
Hematopoietic cell lineage
Apelin signaling pathway
Osteoclast differentiation
TNF signaling pathway
ECM-receptor interaction
IL-17 signaling pathway
Complement and coagulation cascades
B cell receptor signaling pathway
Amyotrophic lateral sclerosis (ALS)
Cocaine addiction
pvalue
Gene Count
C
Biological Process
Cellular Component
Molecular Function
Gene Ratio
blood vessel morphogenesis
regulation of cytokine production
regulation of cell activation
positive regulation of locomotion
transmembrane receptor protein tyrosine kin...
negative regulation of protein phosphorylat...
ossification
regulation of cytoskeleton organization
regulation of homeostatic process
negative regulation of growth
regulation of neuron apoptotic process
eye development
response to lipopolysaccharide
second-messenger-mediated signaling
extracellular matrix organization
extracellular structure organization
vascular process in circulatory system
response to hypoxia
protein kinase B signaling
regulation of synaptic plasticity
negative regulation of developmental growth...
stem cell proliferation
endothelial cell proliferation
regulation of G-protein coupled receptor pr...
regulation of protein import
regulation of reproductive process
chemokine-mediated signaling pathway
non-canonical Wnt signaling pathway
catecholamine metabolic process
catechol-containing compound metabolic proc...
cGMP metabolic process
somatic stem cell population maintenance
forebrain neuron development
convergent extension
osteoblast proliferation
external side of plasma membrane
extracellular matrix
proteinaceous extracellular matrix
axon part
blood microparticle
perikaryon
condensed nuclear chromosome, centromeric r...
cytokine receptor binding
transcription factor activity, RNA polymera...
heparin binding
growth factor activity
integrin binding
collagen binding
fibronectin binding
extracellular matrix binding

Figure S2. RNA-Sequencing Analysis of *mdx* Hearts. (**A**) Volcano plot depicting differentially expressed genes in vehicle-treated *mdx* hearts relative to wild-type hearts. (**B**) Kyoto Encyclopedia of Genes and Genomes enrichment analysis of pathways activated in vehicle-treated *mdx* hearts. (**C**) Gene Ontology enrichment analysis of biological processes, cellular components, and molecular function of CDC-treated *mdx* hearts.

Fig. S3

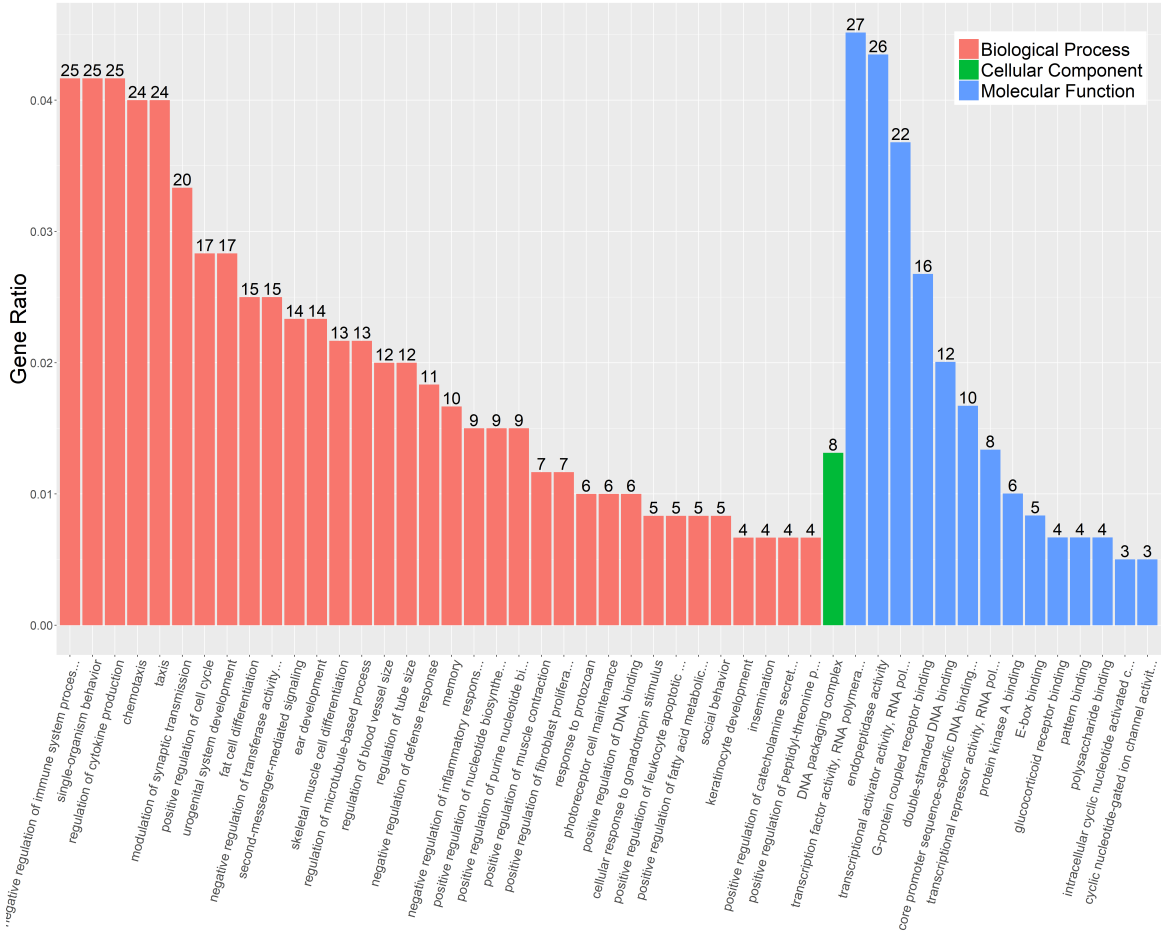
Gene Ratio
0.00
0.01
0.02
0.03
0.04
Biological Process
Cellular Component
Molecular Function
25 25 25 24 24 20 17 17 15 15 14 14 13 13 12 12 11 10 9 9 9 7 7 6 6 6 5 5 5 5 4 4 4 4 8 27 26 22 16 12 10 8 6 5 4 4 4 3 3
negative regulation of immune system proces...
single-organism behavior
regulation of cytokine production
chemotaxis
taxis
modulation of synaptic transmission
positive regulation of cell cycle
urogenital system development
fat cell differentiation
negative regulation of transferase activity...
second-messenger-mediated signaling
ear development
skeletal muscle cell differentiation
regulation of microtubule-based process
regulation of blood vessel size
negative regulation of defense response
regulation of tube size
memory
negative regulation of inflammatory respons...
positive regulation of nucleotide biosynthe...
positive regulation of purine nucleotide bi...
positive regulation of muscle contraction
regulation of fibroblast prolifera...
response to protozoan
photoreceptor cell maintenance
positive regulation of DNA binding
cellular response to gonadotropin stimulus
positive regulation of leukocyte apoptotic ...
positive regulation of fatty acid metabolic...
social behavior
keratinocyte development
insemination
positive regulation of catecholamine secret...
positive regulation of peptidyl-threonine p...
DNA packaging complex
transcription factor activity, RNA polymera...
endopeptidase activity
transcriptional activator activity, RNA pol...
G-protein coupled receptor binding
double-stranded DNA binding
core promoter sequence-specific DNA binding
transcriptional repressor activity, RNA pol...
protein kinase A binding
E-box binding
glucocorticoid receptor binding
pattern binding
polysaccharide binding
intracellular cyclic nucleotide activated c...
cyclic nucleotide-gated ion channel activit...

Figure S3. RNA-Sequencing Analysis of EXO Treated *mdx* Hearts. Gene Ontology enrichment analysis of biological processes, cellular components, and molecular function of EXO-treated *mdx* hearts.

Fig. S4

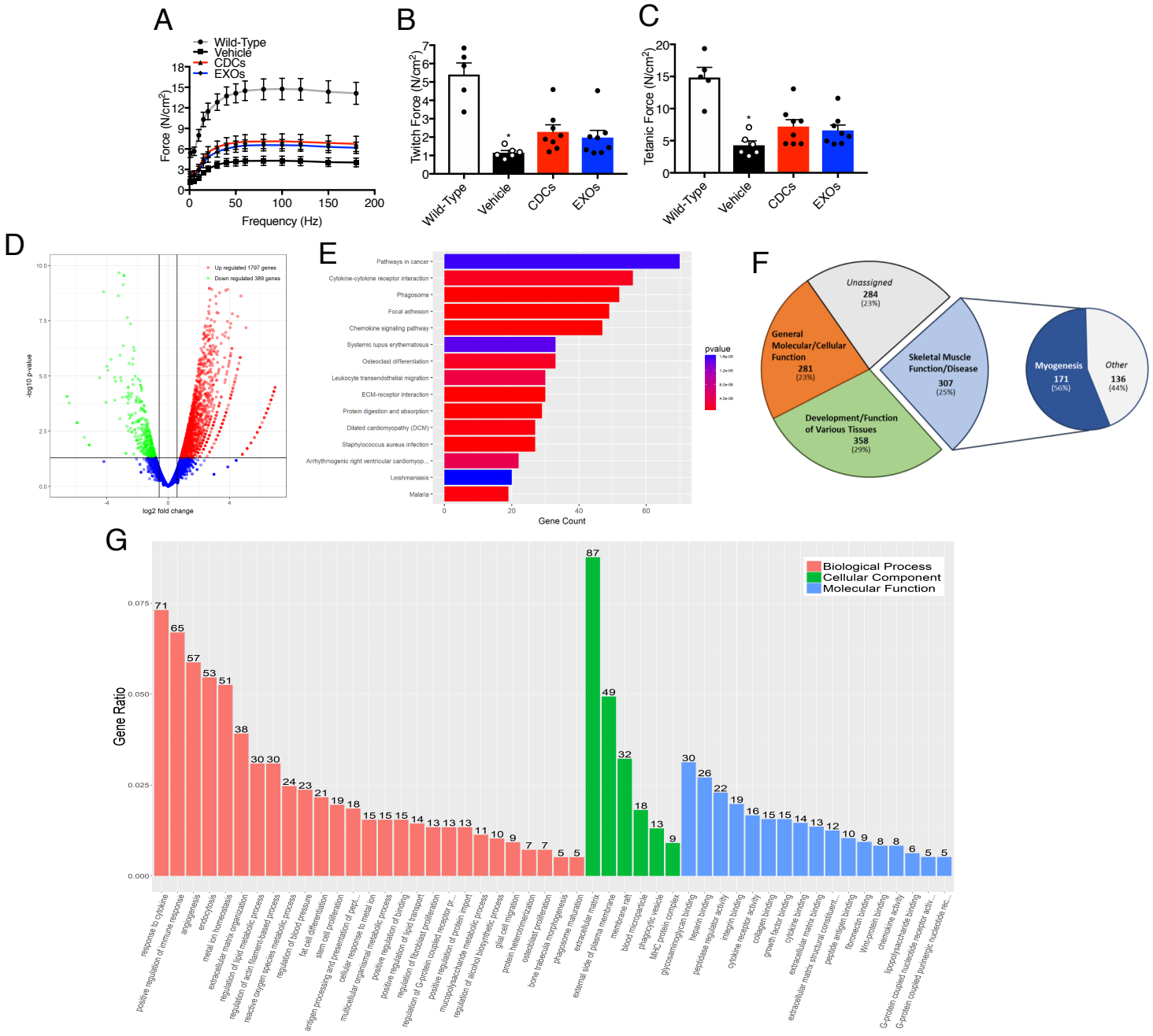
A
Wild-Type
Vehicle
CDCs
EXOs
Force (N/cm²)
Frequency (Hz)
B
Twitch Force (N/cm²)
Wild-Type
Vehicle
CDCs
EXOs
C
Tetanic Force (N/cm²)
Wild-Type
Vehicle
CDCs
EXOs
D
Up regulated 1797 genes
Down regulated 389 genes
-log10 p-value
log2 fold change
E
Pathways in cancer
Cytokine-cytokine receptor interaction
Phagosome
Focal adhesion
Chemokine signaling pathway
Systemic lupus erythematosus
Osteoclast differentiation
Leukocyte transendothelial migration
ECM-receptor interaction
Protein digestion and absorption
Dilated cardiomyopathy (DCM)
Staphylococcus aureus infection
Arrhythmogenic right ventricular cardiomyop...
Leishmaniasis
Malaria
pvalue
Gene Count
F
Unassigned
284
(23%)
General Molecular/Cellular Function
281
(23%)
Skeletal Muscle Function/Disease
307
(25%)
Development/Function of Various Tissues
358
(29%)
Myogenesis
171
(56%)
Other
136
(44%)
G
Biological Process
Cellular Component
Molecular Function
Gene Ratio
response to cytokine
positive regulation of immune response
angiogenesis
endocytosis
metal ion homeostasis
extracellular matrix organization
regulation of lipid metabolic process
regulation of actin filament-based process
reactive oxygen species metabolic process
regulation of blood pressure
fat cell differentiation
stem cell proliferation
antigen processing and presentation of pept...
cellular response to metal ion
multicellular organismal metabolic process
positive regulation of metabolic process
positive regulation of binding
regulation of lipid transport
regulation of fibroblast proliferation
regulation of G-protein coupled receptor pr...
positive regulation of G-protein coupled receptor pr...
positive regulation of protein import
mucopolysaccharide metabolic process
regulation of alcohol biosynthetic process
glial cell migration
protein heterotrimerization
osteoblast proliferation
bone trabecula morphogenesis
phagosome maturation
external side of plasma membrane
extracellular matrix
membrane raft
blood microparticle
phagocytic vesicle
MHC protein complex
glycosaminoglycan binding
heparin binding
peptidase regulator activity
integrin binding
cytokine receptor activity
collagen binding
growth factor binding
cytokine binding
extracellular matrix binding
extracellular matrix structural constituent...
peptide antigen binding
fibronectin binding
Wnt-protein binding
chemokine activity
lipopolysaccharide binding
G-protein coupled nucleotide receptor activ...
G-protein coupled purinergic nucleotide rec...

Figure S4. Biological Effects of CDC or EXO Treatment in *mdx* Mouse Skeletal Muscle. (**A**) In vitro force-frequency relationship of wild-type, vehicle, CDC-, and EXO-treated *mdx* diaphragms (n = 5 – 8 per group). CDC treatment shifted the force-frequency curve up and to the left. (**B**) Twitch and (**C**) tetanic force derived from **A** demonstrate CDC and EXO treatment boosts the developed force by *mdx* diaphragms (n = 5 – 8 per group). (**D**) Colorimetric analysis of protein-carbonyl adducts reveal normalization by CDC treatment in *mdx* solei (n = 7 – 8 per group). (**E**) Volcano plot depicting differentially expressed genes in vehicle-treated *mdx* solei relative to wild-type solei. (**F**) Kyoto Encyclopedia of Genes and Genomes enrichment analysis of pathways activated in vehicle-treated *mdx* solei. (**G**) Custom pathway analysis using IPA assigning genes differentially expressed by CDC treatment in *mdx* solei. (**H**) Gene Ontology enrichment analysis of biological processes, cellular components, and molecular function of EXO-treated *mdx* solei. Statistical significance was determined by Analysis of Variance (ANOVA) with $p \leq 0.05$. When appropriate, a Newman-Keuls correction for multiple comparisons was applied. *statistically different from baseline, #statistically different from vehicle.

Fig. S5

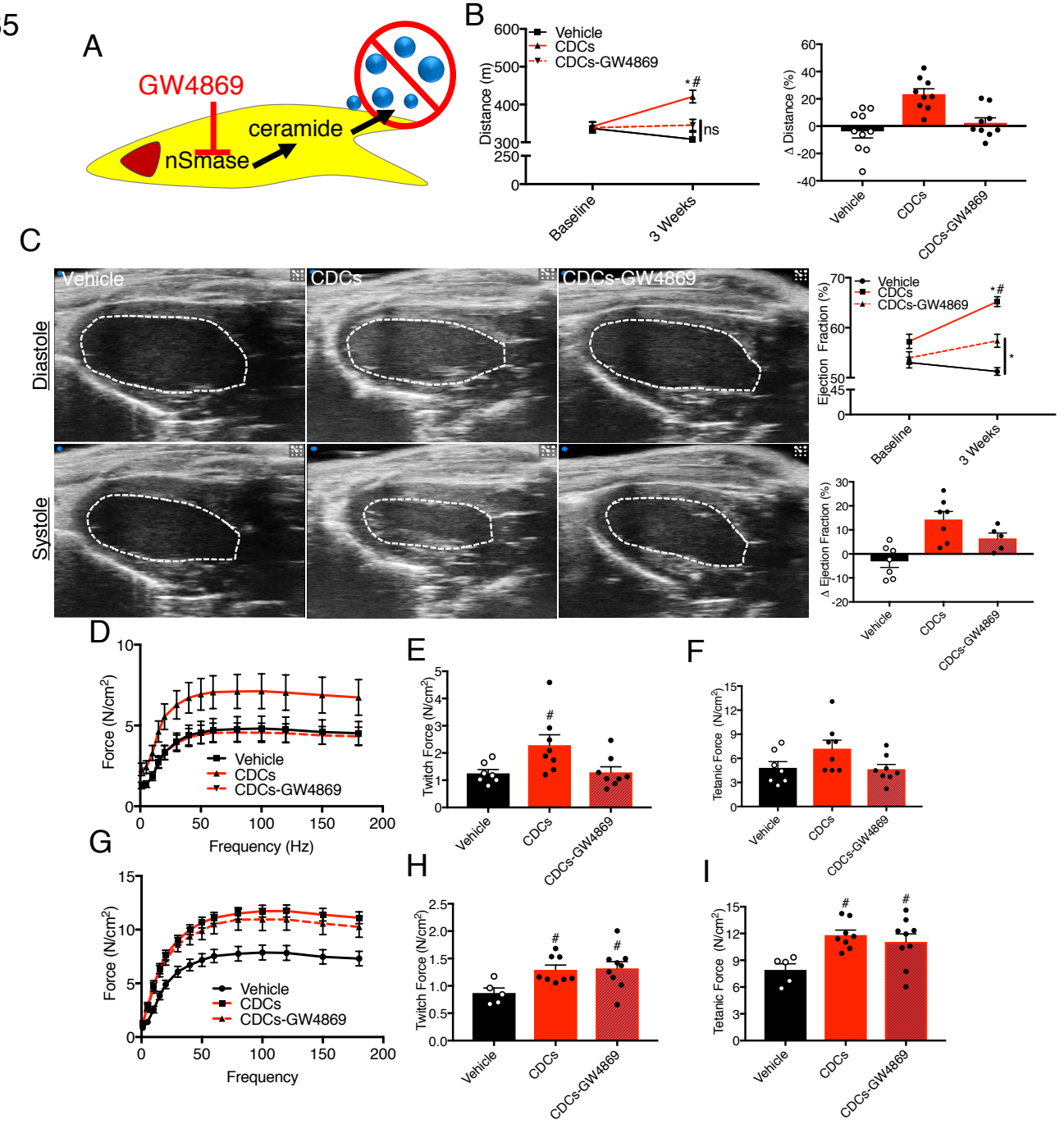
A
GW4869
ceramide
nSmase
B
Vehicle
CDCs
CDCs-GW4869
Distance (m)
*#
ns
Baseline
3 Weeks
Δ Distance (%)
C
Vehicle
CDCs
CDCs-GW4869
Diastole
Systole
Ejection Fraction (%)
Δ Ejection Fraction (%)
D
Force (N/cm²)
Frequency (Hz)
E
Twitch Force (N/cm²)
F
Tetanic Force (N/cm²)
G
Frequency
H
I

Figure S5. Inhibition of Exosome Biosynthesis Renders CDCs Ineffective. (**A**) Schematic of exosome biosynthesis blockade. (**B**) Exercise capacity, as determined by a graded exercise test, was not improved in CDC-GW4869 treated *mdx* mice after 3 weeks (n = 8 – 10 per group). (**C**) Representative echocardiogram tracings. Cardiac function, as measured by transthoracic echocardiography, was modestly increased in CDC-GW4869 treated *mdx* mice after 3 weeks (n = 5 – 8 per group). (**D**) In vitro force-frequency relationship of wild-type, CDC, and CDC-GW4869 treated *mdx* diaphragms (n = 5 – 8 per group). (**E**) Twitch and (**F**) tetanic force derived from **D** demonstrate that GW4869 blocks the functional improvements of CDCs in the *mdx* mouse diaphragm. (**G**) *In vitro* force-frequency relationship of wild-type, CDC, and CDC-GW4869 treated *mdx* solei (n = 5 – 9 per group). (**H**) Twitch and (**I**) tetanic force derived from **G** demonstrate that GW4869 does not block the functional improvements of CDCs in the *mdx* mouse soleus. Bar graphs depict mean ± SEM. Statistical significance was determined by an analysis of variance (ANOVA) with $p \leq 0.05$. When appropriate, a Newman-Keuls correction for multiple comparisons was applied. *statistically different from baseline, #statistically different from vehicle. The vehicle control and CDC-treated data are shared from figures in the main text and supplement, but experiments were conducted contemporaneously. Comparisons were made between three groups.

Fig. S6

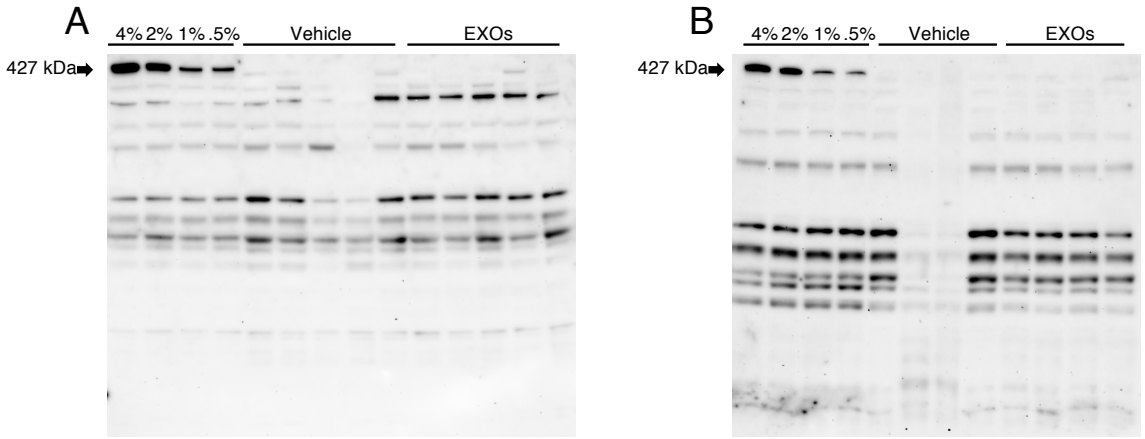

Figure S6. Dystrophin expression in EXO-treated *mdx* skeletal muscle. Immunoblot of the full-length dystrophin protein in the *mdx* soleus (**A**) and diaphragm (**B**). 4 – 0.5% represents a titration of wild-type dystrophin levels for each muscle.